Supporting information

Synthetic and Characterization Methods

A series of pyrolyzed PAN based materials which differ in the formation method, carbonization temperature, composition and dispersity were synthesized.

The electrospun PAN mats were carbonized under vacuum of 10^{-5} Torr at 600 – 2800 ^{o}C for 1-2 h. These materials are referred to as PAN-**t** where **t** is carbonization temperature in ^{o}C. The mass loss during the PAN pyrolysis increases with the temperature increase and composes 40-48 wt% at 750 ^{o}C; 52 wt% at 900 ^{o}C; 55 wt% at 1050 ^{o}C and 57 wt% at 1200 ^{o}C.

All the electrospinning procedures were performed from DMF solutions. For all types of materials, the oxidative treatment in air (heating rate 3 ^{o}C / min) at 250 – 350 ^{o}C for 2 h preceded the carbonization step.

The process of platinum nanoparticle deposition on the treated PAN-1200 mats was performed in two different ways, both ways are quantitative. The first one was to wet a sample (square mat with area of 6.76 cm^2) of PAN-1200 CNFP with hexachloroplatinic acid solution in 0.8 mL of ethanol-water mixture (1:1 v:v). After evaporation of solvent under air, the mat was heated at 280 ^{o}C under vacuum for 1 hour to achieve Pt reduction. The second way was to place PAN-1200 mat into ~10 mL of aqueous solution of calculated amount of hexachloroplatinic acid ($H_2[PtCl_6]$) with 0.5 mL of formic acid (HCOOH) as reducing agent at room temperature for 4-5 days. As we understand the process, in the dilute solution of $H_2[PtCl_6]$ in water with addition of HCOOH, platinum nanoparticle growth is started on the “defects” of carbon structure. Then, Pt is slowly quantitatively reduced and deposited on the nuclei of Pt instead of forming a new nanoparticle. This process leads to the “finger”-like structure of platinum. At the same time, spherical Pt nanoparticles are formed when carbon material is moistured with concentrated solution of $H_2[PtCl_6]$ and treated under vacuum at 280 ^{o}C. Under these conditions, Pt is quantitatively reduced very fast, and for Pt, it is more preferable to form a new nucleus (not necessarily on defects) rather than to be deposited on the already formed nanoparticle. That is why in this case Pt forms small spherical nanoparticles instead of “finger”-like structures. In terms of crystal engineering aspects, we have found that the shape of Pt crystals depends only on the way of Pt deposition (first, from diluted $H_2[PtCl_6]$ solution and, second, from concentrated $H_2[PtCl_6]$ solution with further thermal treatment at 280 ^{o}C under vacuum). We have not found the difference of Pt morphology depending on the thermal treatment temperature of the nanofiber during pyrolysis, despite formation of different chemical surface states of carbon depending on pyrolysis temperature. If to consider a very smooth surface (for example, if a specific

heterocyclic polymer is used as a precursor of nanofiber), slow platinum deposition from dilute $H_2[PtCl_6]$ solution proceeds with difficulties (requires longer times or platinum precipitates from the solution on glassware). However, different polymer nanofiber precursor discussions are beyond the scope of this communication. The reported nanofibers possess enough defects to start Pt nanoparticle growth, but their number is not enough to achieve a uniform spherical particle platinum morphology, leading to formation of "finger"-like platinum instead.

The **performance in HT-PEMFC** on PBI-O-Pht membrane when PAN-1200 with spherical Pt morphology (0.7 mg_{Pt}/cm^2, deposition from concentrated solution of $H_2[PtCl_6]$) was used as an anode and BASF P1000 electrode was used as cathode: open-circuit voltage (V_{oc}) 0.857 V; 0.652 V at 0.2 mA/cm^2; and 0.566 V at 0.4 mA/cm^2.

The **elemental content** (C, H, N) of PAN-**t** mats was determined by Elemental Analyzer 1106 (Carlo Erba). Oxygen content was determined as residual.

The **surface content** of PAN-**t** mats was determined by XPS method using Auger-microscope (Vacuum Generators) equipped with CLAM2 device. The vacuum value in analyzer camera was better than 10^{-8} Torr. Al-anode was used as the illumination source with Kα-line energy of 1486.6 eV. Scale calibration was performed using $Cu2p_{3/2}$ 932.6 eV and $Au4f_{7/2}$ 84.0 eV lines of metal samples, purified by ion etching. Peak positions were standardized by the position of carbon C1s peak with the energy of 285.0 eV which could be attributed either to the carbon contaminants from the vacuum pump oil vapour destruction or carbon material under investigation itself. To enlarge the resolution the spectra were measured at the analyzer energy of 20 eV. The full width at half maximum appeared to equal 1.6 eV illustrating the peaks of carbon contaminants and material itself to be close. The thickness of the analyzed layer was no more that 10 nm. Measurement precision for peak position is ±0.3 eV.

Electrical conductivity of the PAN-t mats was determined using LCR E7-8 4-pin digital meter. The sample of 1 cm width was fixed by two copper plates using soft electroconducting carbon cloth gasket. The distance between copper plates was 1.2 cm. The thickness of the sample was measured using eXacto ElektroPhysik device. Final specific electrical conductivity (σ, S/cm) was calculated according to the formula:

$\sigma = L / (R\ d\ w) = 1.2 / (R\ d \cdot 0.0001 \cdot 1) = 12000/(R\ d)$

where R - measured resistance (Ω);

L - length of the sample (1.2 cm);

w - width of the sample (1 cm);

d – thickness of the sample (μm)

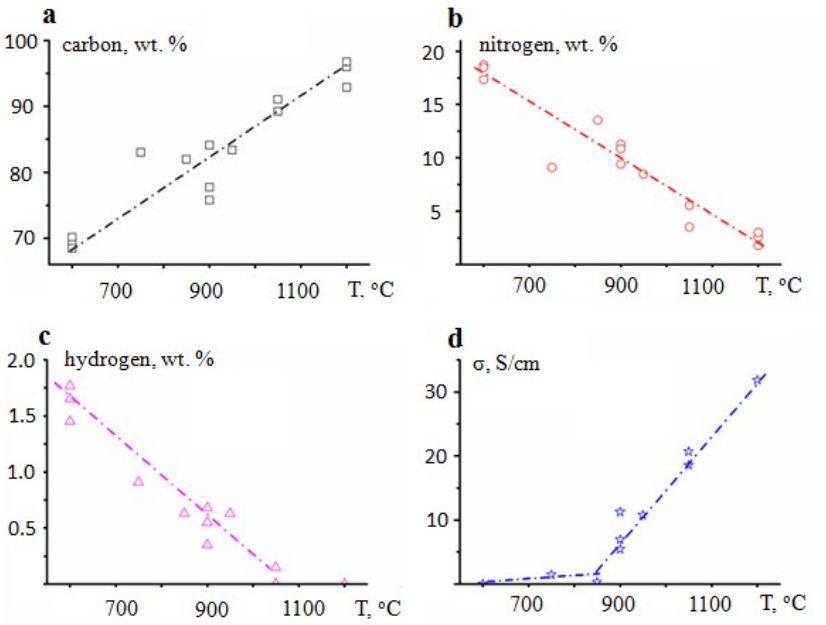

Figure S1. The dependence of carbon (a), nitrogen (b) and hydrogen (c) content, and electrical conductivity (d) vs. the carbonization temperature for PAN-t.

The calculated elemental content of initial PAN homopolymer $(–CH_2\text{-}CH(CN)–)_n$ is 67.9 wt% of carbon, 26.4 wt% of nitrogen and 5.7 wt% of hydrogen. During the oxidative treatment in air the oxygen content increases to such an extent, that even after pyrolysis at 1050 °C under vacuum, the oxygen content exceeds 6 at% in PAN-t surface layer (~10 nm). Oxygen couldn't be removed even after pyrolysis at 2800 °C (Table S1). The effect of the carbonization temperature (600-1200 °C) on PAN-t elemental content, determined by elemental analysis, is shown in Fig. S1 a-c. When the pyrolysis temperature increases, the carbon-enrichment of samples is observed due to the nitrogen, hydrogen and oxygen content decrease. For PAN-t, the carbon content increases up to 68-70 wt% at 600 °C, and up to 92-96 wt% at 1200 °C.

Table 1. The composition and electrical conductivity of PAN-t

№	Sample	Elemental analysis, wt%				σ, S cm^{-1}
		C	N	H	O	
1	**PAN-600**	70.18	17.32	1.65	10.85	0.002
2	**PAN-750**	83.01	9.12	0.91	6.96	1.45
3	**PAN-850**	82.00	13.54	0.63	3.83	0.32
4	**PAN-900**	75.83	11.28	0.68	12.21	5.45
5	**PAN-950**	83.38	8.48	0.63	7.51	10.74
6	**PAN-1050**	89.24	5.55	0.15	5.06	20.65
7	**PAN-1200**	92.85	1.80	0	5.35	31.86
8	**PAN-2800**	99.78	0	0	0.22	324.01

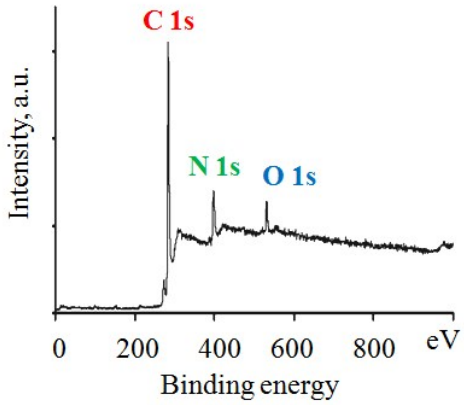

Figure S2. XPS of PAN-900.

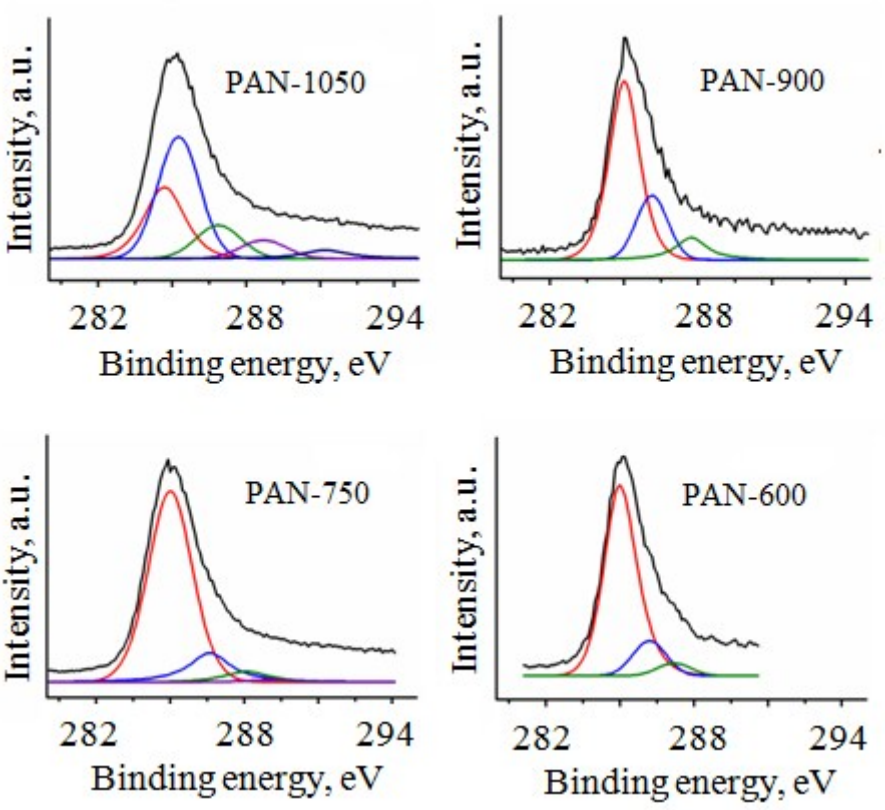

Figure S3. XPS of C1s line for PAN-t.

C1s lines could be deconvoluted giving three most intensive peaks: C1 (285.0±0.3), C2 (286.3±0.3) and C3 (287.2±0.3) eV (Fig. S3). For PAN-1050 it is also possible to determine a line C4 with lower intensity and higher binding energy (291.2±0.3) eV. According to the literature, C1 line corresponds to sp^3- carbon atom [1]; C2 could be assigned to sp^2-carbon bound with nitrogen atom N (-C=N-) or carbon atom (-C=C-) [2]; C3 corresponds to carbonyl and/or quinone group (-C=O) [3]; C4 is a result of π-π^* (band to band) interaction of benzene rings and determines "aromaticity degree" [4]. The absence of 284.4 eV line shows, the most probably, that graphite phase is not formed at 600-1050 ^{o}C. It corresponds to the literature data saying that PAN pyrolysis products are non-graphitizable [5].

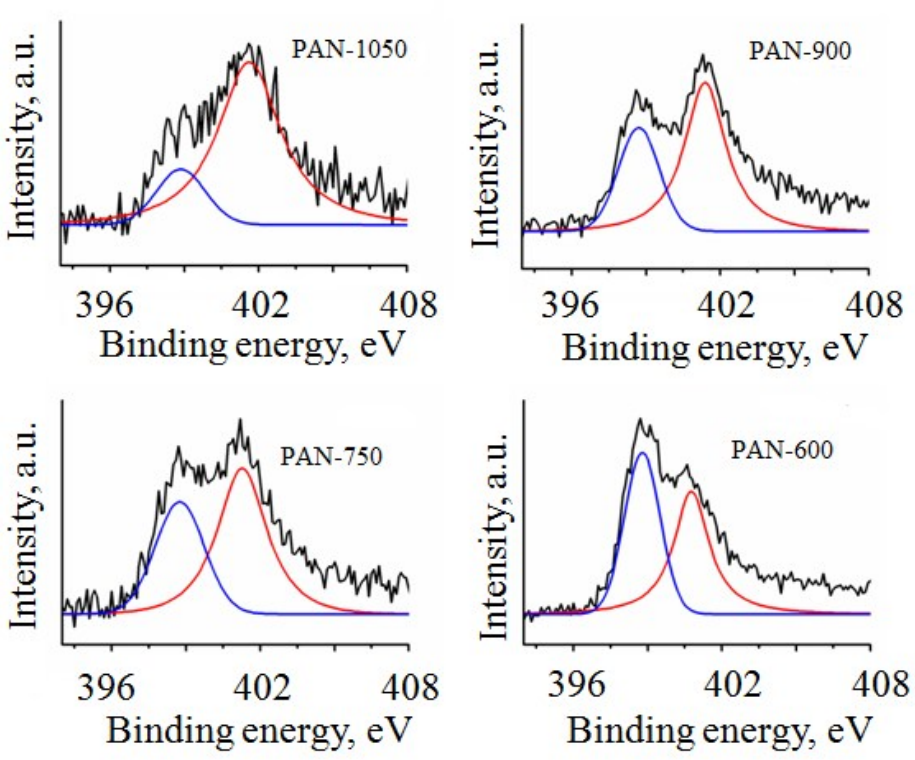

Figure S4. XPS of N1s line for PAN-t.

For all PAN-t samples, N1s lines consist of two lines: N1 (398.7±0.3) eV and N2 (401.0±0.3) eV (**Fig. S4**). The N1 line, which has lower binding energy, corresponds to nitrogen atom in six-member heterocycle on a side plane of the graphene sheet (pyridine form) [2,6]. N2 is shifted relative to N1 on ΔBE = 2 – 2.7 eV, ΔBE increases when pyrolysis temperature increases. N2 corresponds either to graphitic form (where the nitrogen is in six-member heterocycle on a basal surface of the graphene sheet) or to amine form (where the nitrogen is in six-member heterocycle on a side plane of the graphene sheet and bound with hydrogen atom) [2].

Table S2. Surface layer content of PAN-t according to XPS.

Sample	Line	BE, eV	Designation in text	*c*, at%	c_{Σ}, at%	Form
PAN-600	C1s	287.2	C3	4.19	80.84	carbonyls or quinones -C=O
		286.2	C2	11.52		sp^2 -C=C-; -C=N-
		285.0	C1	65.13		sp^3 -C-C-
	N1s	400.8	N2	6.94	13.96	graphite or amine form
		398.8	N1	7.02		pyridine form
	O1s	531.8	-	5.2	5.2	carbonyls or quinones-C=O
PAN-900	C1s	287.4	C3	5.78	85.49	carbonyls or quinones -C=O
		286.4	C2	19.88		sp^2 -C=C-; -C=N-
		285.1	C1	60.53		sp^3 -C-C-
	N1s	401.4	N2	6.49	9.95	graphite or amine form
		398.7	N1	3.46		pyridine form
	O1s	532.9	-	4.56	4.56	carbonyls or quinones -C=O
PAN-1050	C1s	291.1	C4	4.65	88.68	$\pi - \pi^*$ - benzene ring interections
		288.0	C3	6.8		carbonyls or quinones -C=O
		286.3	C2	21.96		sp^2 -C=C-; -C=N-
		285.0	C1	55.27		sp^3 -C-C-
	N1s	401.6	N2	3.86	4.69	graphite or amine form
		398.9	N1	0.83		pyridine form
	O1s	532.6	-	6.64	6.64	carbonyls or quinones -C=O

The concentration of oxygen atoms should be close to C3 atom concentration and this proved by the experimental data (Table S2). C1 concentration is related to electrically non-

conductive carbon phase (sp^3-carbon), its content decreases with the carbonization temperature increase, which, in turn, leads to electrical conductivity increase (Fig. S1 d). The higher the temperature, the lower the nitrogen concentration becomes and the higher N2/N1 ratio is observed: from ~1 at 600 °C to ~4.7 at 1050 °C. Relative depletion of N1 and surface enrichment by N2 could be explained, according to [2], by lower stability of N at side positions (pyridine form) compared with N at central positions (graphitic form). Comparing N1+N2 concentration with C2 one, it is seen that the carbonization temperature increase leads to lower intensity of –C=N- and higher intensity of –C=C– bonds.

XRD data

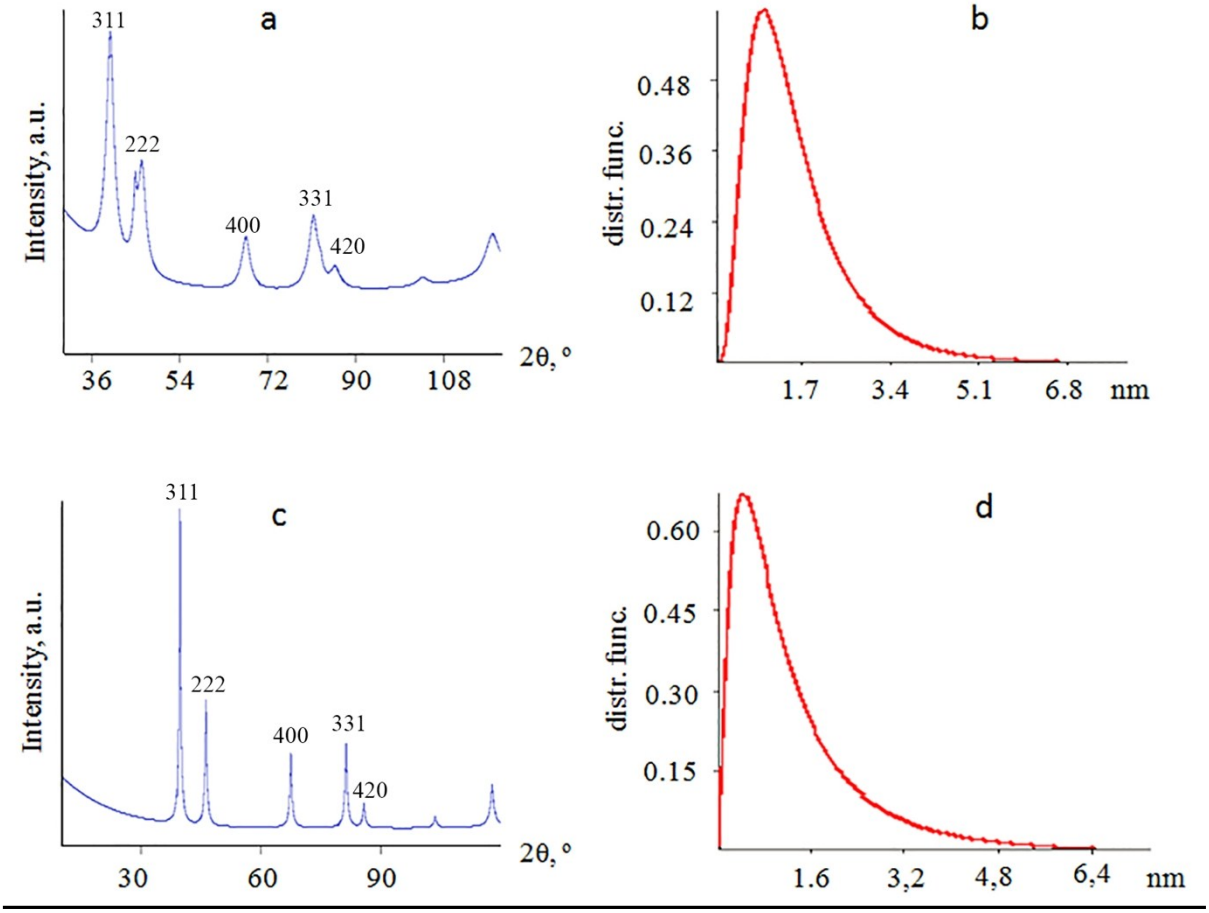

Figure S5. X-Ray diffraction pattern and size distribution curve for PAN-1200 with 20 % Pt (a and b, the second way of Pt deposition), and with 50 % Pt (c and d, the first way of Pt deposition).

Average particle size is 1.48 nm, Scherrer particle size is 11.5 nm.

The particle size distribution is log-normal:

$$f_d(d) = \frac{1}{d\sigma\sqrt{2\pi}} e^{-\frac{(\ln d - \mu)^2}{2\sigma^2}}, d > 0$$

FTIR data

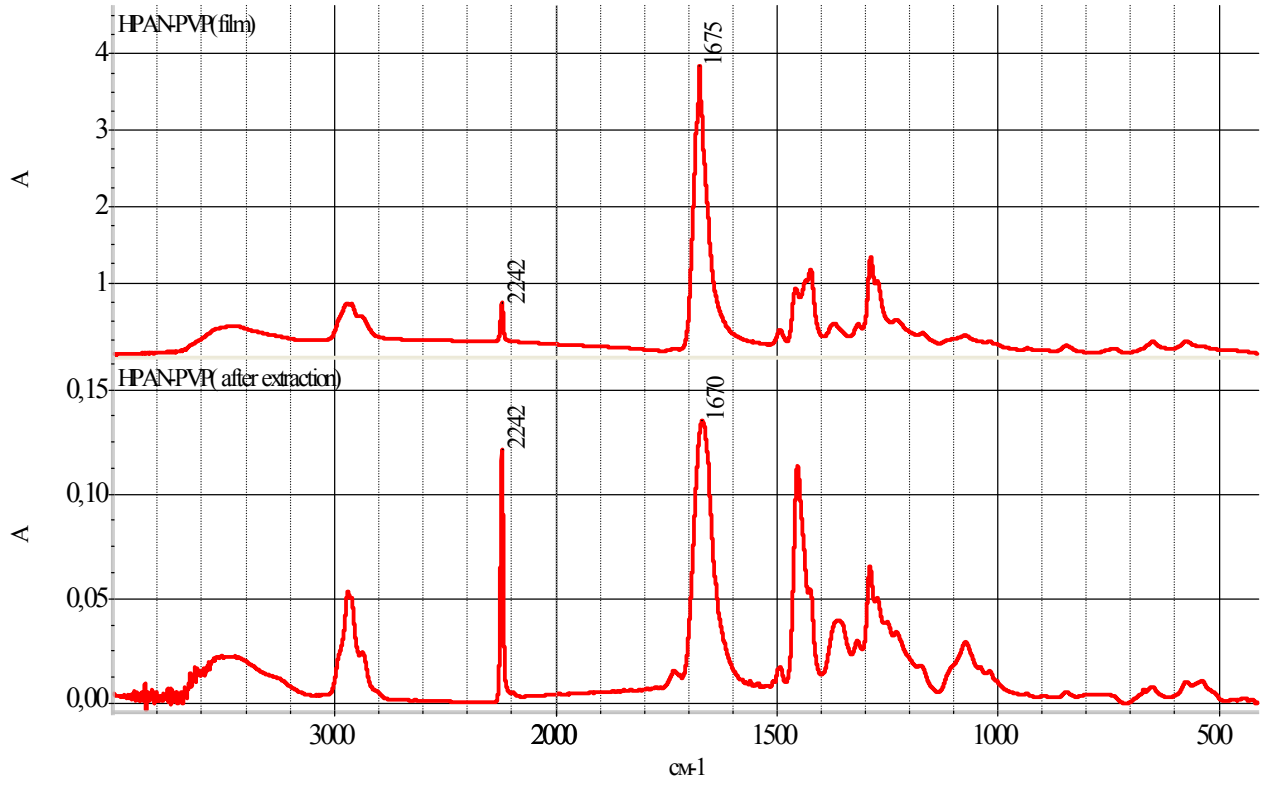

Figure S6. IR-spectra of the PAN/PVP 9:1 mat before (top) and after (bottom) extraction. According to the signals at 2240 cm^{-1} (nitrile group) and 1670 cm^{-1} (carbonyl group) the concentration of PVP has decreased 3-4 times, so that it is < 5 wt.%.

Porosimetry

By using the method of standard contact porosimetry [7,8] the differential pore volume distribution vs. logarithm of pore radius curves were obtained.

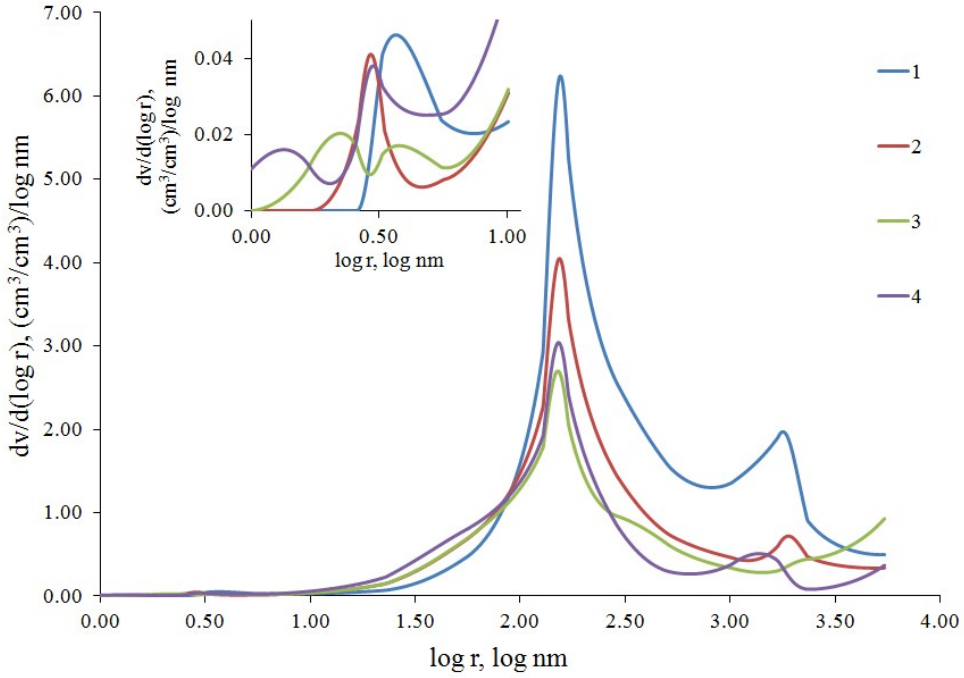

Figure S7. Differential pore volume distribution vs logarithm of pore radius. (Consequent treatment steps of the same material: 1 – initial PAN/PVP nanofibers; 2 – extracted by ethanol to remove PVP; 3 – oxidized at 250 °C in air; 4 – pyrolyzed at 1000 °C under vacuum).

REFERENCES

[1] N.I. Nefedov, X-ray photoelectron spectroscopy of chemical compounds: handbook [in Russian], Moscow, Khimiya, 1984.

[2] G. Soto, E.C. Samano, R. Machorro, F.F. Castillion, M.H. Farias, L. Cota-Araiza, XPS, AES and EELS study of the bonding character in CN_x films, Superf. Vacio 15 (2002) 34.

[3] L.-H. Zhou, Z.-J. Sui, J. Zhu, P. Li, D. Chen, Y.-C. Dai, W.-K. Yuan, Characterization of surface oxygen complexes on carbon nanofibers by TPD, XPS and FT-IR, Carbon 45 (2007) 785.

[4] S. Ye, A.K. Vijh, L.H. Dao, New fuel cell electrocatalyst based on highly porous carbonized polyacrylonitrile foam. The nature of platinum-support interaction, J. Electrochem. Soc. 144 (1997) 90.
[5] P. Morgan, Carbon fibers and their composites, Taylor & Francis, Boca Raton, London, New York, Singapore, 2005.
[6] F. Jaouen, J. Herrannz, M. Lefevre, J.-P. Dodelet, U.I. Kramm, I. Herrmann, P. Bogdanoff, J, Maruyama, T. Naqaoka, A. Garsuch, J.R. Dahn, T. Olson, S. Pylypenko, P. Atanassov, E.A. Ustinov, Cross-laboratory experimental study of non-noble-metal electrocatalysts for the oxygen reduction reaction, ACS Appl. Mater. Interfaces 1 (2009) 1623.
[7] Yu.M. Volfkovich., V.S. Bagotzky, V.E. Sosenkin, I.A. Blinov Colloid. Surface. A. 187 (2001) 349.
[8] Yu.M. Volfkovich, V.E. Sosenkin, V.S. Bagotsky J. Power Sources. 195 (2010) 5429.